

STATIC CHARACTERISTICS OF AN IN-PARALLEL ACTUATED MANIPULATOR FOR CLAMPING AND BRACING APPLICATIONS

Kok-Meng Lee
Assistant Professor

Georgia Institute of Technology
Atlanta, GA 30332

Roger Johnson
Member of Technical Staff, R & D

AT&T Bell Laboratory
Whippany, New Jersey 07981

ABSTRACT

This paper presents the static characteristics of a three degrees of freedom (DOF) in-parallel actuated manipulator and its desired static actuator characteristics for clamping and bracing applications, where the term "bracing" refers to a strategy to rigidize the wrist for subsequent fine-motion performed by the end-effector or a second manipulator. The short-arm manipulator is characterized by its rigidity, high force-to-weight ratio, and relatively simple inverse kinematics. In particular, the paper highlights the influences of the joint reactions on the manipulator performance and suggests appropriate control strategy for clamping and bracing.

1. INTRODUCTION

Recent development in computer-integrated manufacturing (CIM) has provided motivation for re-examining the concept of flexible fixturing systems for processing. In particular, these research efforts have been directed towards labor cost reduction, reduced inventory, and consistent product quality as well as reducing scrap. It has been well recognized that the total machining cost can be significantly reduced with adaptive fixturing of the workpiece in a more cost efficient CIM environment [1-3]. The structured activities, such as unloading of a workpiece from a pallet (workhandling), clamping of a workpiece for machining without damaging or plastically deforming the workpiece (workholding), and subsequent loading of a finished workpiece onto the pallet (workhandling), are pre- and post-requisite activities to the operations. Conceptually, both workholding and workhandling are typical activities of robotic manipulators. With few exceptions the robotic manipulators of today, which are generally open-chain mechanisms, are limited to light loading applications, typically workhandling alone. The attractive possibility of combining both workhandling and workholding using a single manipulator has a significant potential in reducing machine setup time by eliminating a number of intermediate material handling activities.

Speed, accuracy, dexterity, large workspace, and reliability with minimum weight and complexity are some of the performance measure attributes for robotic manipulators. For tasks where the vibratory interaction forces generated between the end-effector and the workpiece are severe, a means of decoupling the fine

motion from gross motion is important to prevent transmission of the vibratory forces through the coupling between the arm and the workpiece-environment interface. A design of a **jig hand**, which was derived from the use of a clamping jig used in machining, was suggested in [4] to bear the vibratory interaction forces during machining operations. A more general strategy, **bracing**, aiming to rigidize the wrist of a light-weight arm for subsequent fine motion was proposed in [5]. As pointed out in [5], bracing is analogous to the human strategy of steadying the hand for precise manipulation such as threading a fibre through the eye of a needle or performing dexterous work such as writing. The principle of jig hand or bracing is to reduce the compliance by over-constraining the manipulator and is to introduce a means for part reference [6].

This paper presents the static characteristics and control strategy of a three DOF in-parallel actuated manipulator as a bracing wrist. The kinematic characteristics of the three DOF actuated manipulator have been presented in [7]. The manipulator is featured with two orientation freedoms to adapt to a complex surface and a translation freedom for clamping. In particular, the paper highlights the influences of the over-constraining forces on the manipulator performance using the presentation of the velocity, and force ellipsoids which were often employed in robotics for prediction of singularity [8], graphical representation of static characteristics, and for optimization of task performance [9].

2. STATIC ANALYSIS

A schematic of the three DOF in-parallel actuated manipulator is shown in Fig. 1, where the moving platform can be manipulated with respect to the base platform by varying the link lengths. To aid the static analysis of the tripod-like mechanism, a local coordinate 123 with unit vector u_j ($j=1,2,3$) is assigned at each of the pin joints and ball joints where the unit vector, $j=2$, is in the direction pointing from the center of the platform towards the joint. The difference in the orientation of the three local axes, which are independent of the platform position, is the 120 degrees rotation about their z axis.

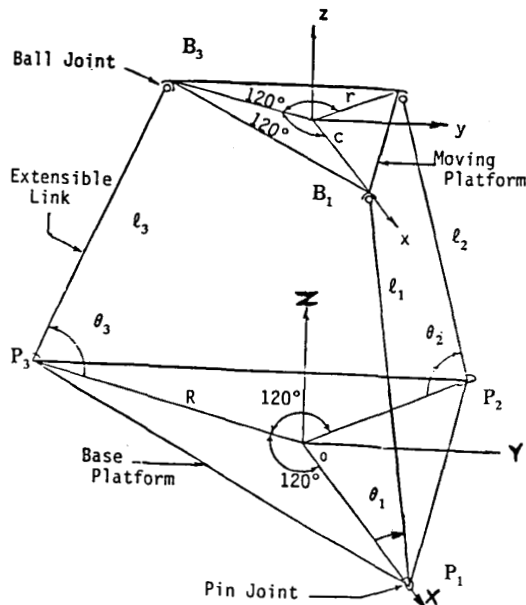


Fig.1 A 3 DOF In-parallel Actuated Manipulator

In the static equilibrium of the i^{th} link, the ball joint is subjected only to three reaction forces as it does not resist any moments within the range of motion. Likewise, the frictionless pin joint does not support a moment about 1-axis. The force balance of the i^{th} link is

$$\sum_{j=1}^3 (F_{ji} - f_{ji}) u_j - W_l u_3 = 0 \quad (1)$$

where F_{ji} and f_{ji} are the components of reaction forces in the direction of j -axis at the i^{th} pin joint and ball joint respectively. The moment balance about the i^{th} pin joint yields:

$$\sum_{j=1}^3 (M_{ji} u_j - r_{li} \times f_{ji} u_j) - r_{mi} \times W_l u_3 = 0 \quad (2)$$

where

$$r_{mi} = Q_i \cos \theta_i u_2 + Q_i \sin \theta_i u_3$$

$$r_{li} = L_i \cos \theta_i u_2 + L_i \sin \theta_i u_3$$

and Q_i = center of gravity of the i^{th} link measured from the i^{th} pin joint,

W_l = weight of each link, and

M_{ji} = moment at the i^{th} pin joint about the j -axis.

Similarly, the static equilibrium of the moving platform in the X, Y, Z directions results:

$$A - W_p u_3 + \sum_{i=1}^3 \sum_{j=1}^3 f'_{ji} u_j = 0 \quad (3)$$

$$\Gamma - \sum_{i=1}^3 \sum_{j=1}^3 (r_i \times f'_{ji} u_j) = 0 \quad (4)$$

where f'_{ji} = reaction force at the i^{th} ball joint along the j^{th} axis w.r.t XYZ coordinate
 A = applied force at the end effector,
 W_p = weight of the platform, and
 r_i = distance vector from the center of the plate to the i^{th} ball joint, and
 Γ = applied moment at the end-effector.

By resolving the vectors into three orthogonal directions, Equations (1) and (2) yield nine equations each. Similarly, six equations can be derived from Equations (3) and (4). The twenty four unknown reaction forces and moments under static conditions can be computed from Equations (1) through (4).

To determine the reaction forces at the ball joints in closed-form, which is an important advantage for real-time computation of the external forces acting on the link, the nine reaction components at the three ball joints can be determined from Equations (2)-(4). From Equation (2), the reaction along 2-axis can be expressed as a function of the corresponding reaction along 3-axis. Also, the reaction of the ball joint along the 1-axis, f_{1i} , can be determined in terms of those along the 2- and 3-axes from three simultaneous equations, Equation (3) with $j=1,2$ and Equation (4) with $j=1$. With the components along 1-axis and 2-axis expressed as functions of that along 3-axis, the latter can be determined directly from the three remaining equations, Equation (3) with $j=3$ and and Equation (4) with $j=2,3$ respectively.

As the link is constrained to move in a plane motion, only the reaction components, f_{1i} and f_{3i} , appear explicitly in the link dynamic equations. The components of f_{1i} and f_{3i} along the link are essentially the thrust load to the actuator and that perpendicular to the link provide the θ -motion. However, the reaction force perpendicular to the plane of motion of the link must be supported by the pin joint, which tends to increase the joint friction. Since real joints are often a source of compliance, a bending moment on the link would result in a static deflection and an increase of stiction in both the revolute and the prismatic joints.

3. VELOCITY AND FORCE ELLIPSOIDS

The manipulator is structurally designed to control the axial loads along the links and the moments about the x and y axes. However, when the degree of joint space is less than that of the task space, there are certain directions in which the actuator cannot exert a static force as desired and in which the force/torque must be supported through the reactions at the joints. The reaction at the joints would initiate a cantilever bending moment on the links which generates a deflection and an increase in stiction and friction on the prismatic joint along the link. To gain a better insight to the static characteristics, the concepts of velocity and force ellipsoids are employed.

Transmission Ratios: The closed-form inverse kinematic is of the form: $L = f(X)$ where $L = [L_1, L_2, L_3]^T$ and $X = [X, Y, Z]^T$ are the joint and task coordinate vectors. A 3×3 Jacobian matrix, $J(X)$, which relates the joint velocity to the task velocity is defined as

$$\dot{L} = J(X)\dot{X} \quad \text{where} \quad J_{i,j} = \partial L_i / \partial X_j \quad (5)$$

The unit sphere is defined by:

$$\|\dot{L}\|^2 = \dot{L}^T \cdot \dot{L} = \dot{L}_1^2 + \dot{L}_2^2 + \dot{L}_3^2 \leq 1$$

and is mapped into an ellipsoid by

$$\dot{X}^T (J^T J) \dot{X} \leq 1$$

The principal axes of the ellipsoid coincide with the three eigenvectors of $(J^T J)$. The eigenvectors are denoted as A, B, C vectors, where $|A| > |B| > |C|$. The length of the principal axes is equal to the reciprocal of the square root of the corresponding eigenvalue. The velocity transmission ratio (VR) along a particular direction of interest is defined as

$$VR = \{U^T (J^T J) U\}^{1/2} \quad (6)$$

where U is a unit vector in the direction of interest. A graphical representation of VR is shown in Fig. 2(a). From the principle of virtual work, the corresponding force ellipsoid is defined by $\Gamma^T (J^T J)^{-1} \Gamma \leq 1$ where Γ is the external force vector acting at the center of the moving platform, and the force transmission ratio:

$$FR = \{U^T (J^T J)^{-1} U\}^{1/2} \quad (7)$$

The underlying assumption is that the force ellipsoid is derived on the basis of an ideal transformer and that external torques acting on the moving platform are not accountable by Equation (7). The principle axes of the velocity and force ellipsoids coincide, but the square of the force transmission ratio is inversely proportional to that of the velocity transmission ratio. The three perpendicular eigenvectors determine the orientation of the ellipsoid which depicts the velocity transmission ratio of the manipulator.

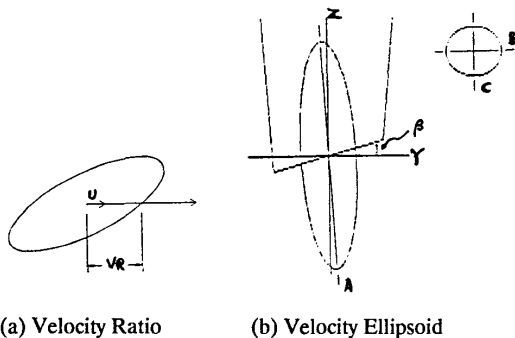


Fig.2 Graphical Display of Velocity Ellipsoid

A typical configuration is shown in Fig. 2(b). It is noted that both B and C vectors along the minor axes are of the same order of magnitude but are much smaller than that of the A-vector. Also, the volume of the velocity ellipsoid decreases as the platform ratio, r/R decreases. The optimal direction for effecting velocity is along the major axis where the velocity transmission ratio is a maximum. It also implies that the force transmission ratio is a minimum, and active force control can be more accurately controlled in this direction. Conversely, the force transmission ratio is a maximum along the minor axes of the velocity ellipsoid, where the forces acting along these axes are supported primarily by the shared reactions at the joints. Although the velocity control can be more accurately controlled along the minor axes of the velocity ellipsoid, the translational freedoms along the minor axes have a very limited working range and can be achieved only at a sacrifice of orientation freedoms [7].

4. APPLICATION EXAMPLES

As the manipulator is structurally designed to control the axial loads along the links and the moments about the x and y axes, any external forces acting along the minor axes of the velocity ellipsoid would initiate a cantilever bending moment on the links. The bending moment can be effectively minimized if the maximum instantaneous velocity transmission ratio (or minimum force transmission ratio) along a particular direction is chosen.

Example 1: Clamping Mechanism

Consider a three DOF in-parallel actuated manipulator with a loadable vacuum gripper performing a clamping operation. The manipulator, after unloading the workpiece from the pallet, is required to exert a clamping force onto the workpiece for subsequent operation at a specified configuration.

For a configuration where the Euler angles (α, β, γ) of the moving platform [7], $\alpha = \beta = 0$, the velocity ratio is equal to $\sin\theta/\sqrt{3}$ along the Z-axis and is zero along both X and Y axes although the moving platform is free to rotate about the x and the y axes at this particular configuration. This also implies that the force transmission is infinite in X and Y directions and that any external forces in X and Y directions are supported structurally by the shared reactions at the joints. This result is independent of the platform ratio, r/R . However, the control of position and force in X- and Y-directions is not possible at $\alpha = \beta = 0$.

If instead, the manipulator is required to exert a clamping force along the z-axis of the moving platform on a fixture at an angle of 20° . It is of interest to determine an optimal α when $\beta = 20$ degrees, which would result in a minimum bending moment on the link. The force transmission ratio as a function of α for $\beta = 20$ degrees is computed and is displayed in Fig. 3, where $Z = 0.42m$ (1.4 feet). Due to the evenly spaced ball joints, the force ratio has three local maximums at $\alpha = 0, 120,$ and 240 degrees and three local minimum at $\alpha = 60, 180$ or 300 degrees. As discussed previously, the minimum bending moment

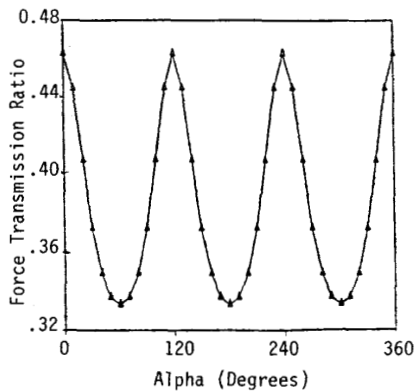
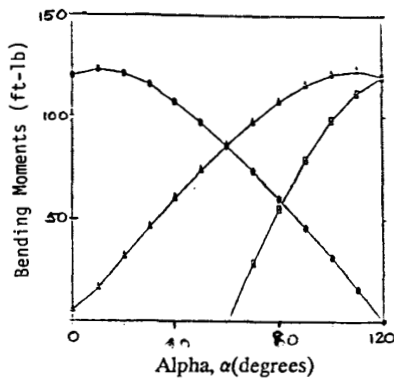
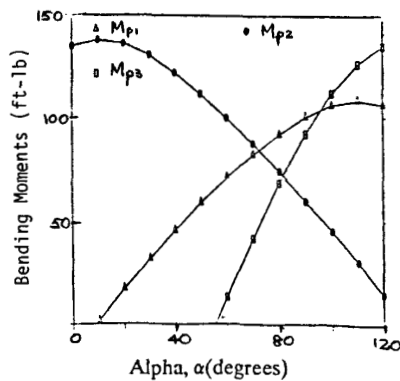


Fig. 3 FR in the Direction of z-axis



(a) Bending Moment of Clamping Example ($\beta=20^\circ$)



(b) Bending Moment of Drilling Example ($\beta=20^\circ$)

Fig. 4 Computed Bending Moments on the Links

on the link is corresponding to the minimum force ratio at $\alpha=60, 180$ and 300 degrees.

Example 2: Machining

As Equation (7) does not account for the influences of external torques, the maximum velocity ratio corresponds to the preferred posture for a pure translational load. The comment is illustrated with the following drilling example. Instead of clamping, the manipulator is used to drill an aluminum fixture at a 20 degree angle. The twist drill exerts a cutting torque of 6.775 N-m (5 foot-pounds) about the z-axis and a thrust force of 1335 N (300 pounds) along the z-axis while drilling at a pre-determined constant feedrate. Again, it is of interest to determine an optimal α when $\beta = 20$ degrees, which would result in a minimum bending moment on the link. Although the velocity ratio as a function of α when $\beta = 20^\circ$ is essentially the same as that of Example 1, the bending moments on the link for a thrust load of 1335 N with and without the cutting torque were significantly different.

The computed results using the static algorithm are plotted in Fig. 4, where the weight of the moving platform is assumed to be negligible in the computation for simplicity. As the plane of motion of the links is in parallel to the direction of gravity, the weights of the extensible links have no effects on the bending moments. The bending moments at $\alpha=60^\circ, \beta=20^\circ$ and $Z=0.42$ m are computed to be $116, 116, 0$ N-m ($80, 80, 0$ ft-lbs) and $96.2, 135.5, 19.24$ N-m ($71, 100, 14$ ft-lbs) corresponding to with and without the applied torque about z-axis of 6.775 N-m. As indicated in the results of the static analysis, the maximum bending moment on the link can be significantly reduced by operating α at 70° . The corresponding bending moments are $116, 116, 67.75$ N-m ($80, 80, 50$ ft-lbs), where the twist moment is shared primarily by the third link. The reactions at both pin and prismatic joints would increase the stiction to the joint motion, which must be compensated in the trajectory control in line with the feedrate.

Example 3: Bracing with light-weight link

Coarse motion robotic arms characterized by their large workspace envelope, dexterity, and high force-to-inertia ratio are open-chain mechanisms associated with long but light-weight links, which usually have poor static accuracy and mechanical stiffness due to its cantilever-like configuration. An effective solution to improve the static accuracy and to increase the system bandwidth using a bracing strategy was proposed in [12]. The general bracing strategy consists of three stages. The first stage involves the coarse positioning of the lightweight arm subjected to a relatively large degree of uncertainty due to some unaccountable system errors. The second stage is to rigidize the end-point of the coarse motion arm to achieve high bandwidth, which is limited by the natural frequency. The third stage involves the end-effector, or a second manipulator performing its fine-motion task.

The manipulator which has two DOF orientation motion and a translational clamping, gripping, or attaching motion provides an effective means of bracing at the wrist. The potential increase in system bandwidth by bracing can be readily demonstrated by comparing the natural frequency of a one-dimensional thin rod with both ends clamped and that of a thin rod with one end clamped and the other end free. The former is inversely proportional to the length whereas the latter is inversely proportional to the square of the length.

5. CONTROL STRATEGY OF BRACING WRIST

With the inertia of the moving platform and the payload on the individual link considered as reaction forces acting at the ball joints, the moving platform can be controlled by modulating the link actuation. The control of the bracing wrist can be divided into three distinct phases, namely, coarse positioning, compliant adapting and force control of the moving platform. An approach based on the static characteristics contouring to approach that of the ideal actuator is suggested.

Characteristic Contouring. The type of actuator which one uses depends on the load requirements. Ideally, if forces or torques on the load are to be regulated, a variable pure force source independent of velocity is desired. On the other hand, if the velocity or position of a load is to be regulated, a variable pure velocity or position source independent of the force is desired. In position control of inertial systems, velocity controlled actuators are commonly used. An ideal actuator should be capable of functioning as an ideal orientation or torque actuator or have the ability to contour the output characteristics to adapt the loading conditions. Real physical systems, however, possess certain dynamic and frictional effects and have limited power capability. Also, a physical system which is simultaneously characterized as an ideal position/orientation and as an ideal force/torque actuator is, in fact, non-existent.

The strategy to shape the output characteristics of a fluidic servovalve to adapt to load specifications was addressed in [10] and was later demonstrated in hydraulic position servo in [11]. Without loss of generality, the steady-state equation of a typical actuator with saturation can be approximated by Equation (8) as shown in Fig. 5(a).

$$\tau = \tanh \tau_{act} \cdot \omega \quad (8)$$

where τ , τ_{act} , and ω are the external torque, the actuating torque and the actuator speed normalized to their saturation values respectively. With the τ_{act} defined by Equation (9)

$$\tau_{act} = K_1 i + K_2 \tau + K_3 \omega \quad (9)$$

the steady-state solution of the closed-loop actuator system is

$$\tau + \omega = \tanh [K_1 i + K_2 \tau + K_3 \omega] \quad (10)$$

where i is the reference input normalized to its maximum value, i_{max} .

To achieve the link actuation characteristics approaching that of the ideal actuation, the gains are chosen so that the controlled variable is feedback negatively and the complementary power variable is feedback positively. The effect of negative feedback tends to decrease the incremental gain which is defined as $\{\partial \tau / \partial i\}_{i=0, \omega=0}$ or $\{\partial \omega / \partial i\}_{i=0, \tau=0}$ to achieve a wide range of linearity. On the other hand, the positive feedback results in increasing the incremental gain about the origin. Ideally, the force incremental gain $\partial \tau / \partial i|_{i=0, \omega=0}$ for velocity control is infinite so that the stiction can be overcome. Similarly, the ideal velocity incremental gain $\partial \omega / \partial i|_{i=0, \tau=0}$ for force control is infinite so that the theoretical instantaneous response can be achieved. A typical steady state characteristic represented by Equation (10) is shown in Fig. 5(b).

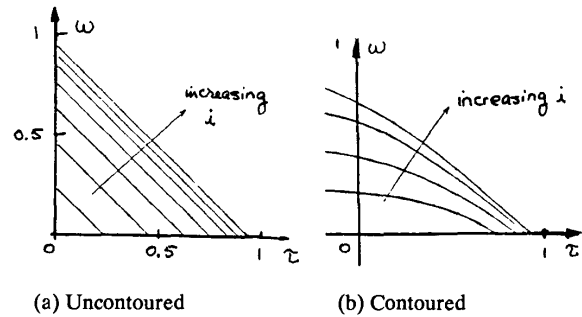


Fig. 5 Output Characteristics

Linearized Actuator Servo. Fig. 6 shows the realization of a position servo where the actuating torque is feedback positively. If the feedback gains are selected to $K_a K_m$ exactly, an infinite forward gain in the velocity servo would result.

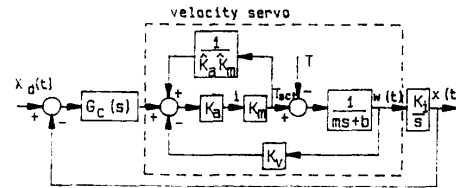


Fig. 6 Position servo

To avoid jamming or damage in the presence of uncertainties, some means of compliance are often added to the manipulator. Active compliance can be achieved by impedance control strategy [13], where the desired equivalent impedance of the link actuation, $Z_d(s)$, to be generated is of the form:

$$\frac{F_e}{\Delta V} = Z_d(s)$$

where $F_e = Z_e V$, $\Delta V = i - V$, s is a Laplacian operator, and $Z_e(s)$ is the environment impedance. Fig. 7 shows an ideal impedance and force control scheme suggested by Goldenbery [14].

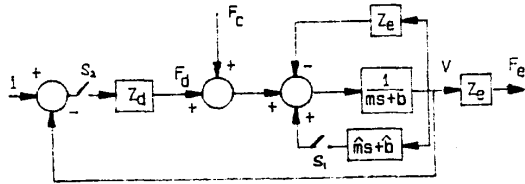


Fig. 7 Force and Impedance Control

To realize the ideal impedance or force control, the positive feedback parameters must be selected to be m and b exactly. S_1 is a contact sensing switch and is opened when $F_e = 0$. The ideal impedance control and force control are achieved by closing and opening the switch S_2 respectively. When $F_e = 0$ and S_2 closed, a force, F_d , is generated at the output of the impedance controller ($F_d = \Delta V \cdot Z_d$) and is equal to F_e due to the ideal actuator characteristics.

Implementation Issues. The incremental gain of a positive feedback system is sensitive to uncertainties. Since the actuator dynamic model is generally not known exactly, the gains must be selected with great care to avoid a negative incremental gain. Furthermore, the need to positive feedback both the velocity and acceleration in the impedance and control scheme may result in an unstable force control. Therefore, $[(m-\hat{m})/(b-\hat{b})]$ and $(b-\hat{b})$ must both be positive.

CONCLUSION

The static characteristics of a three degree of freedom in-parallel actuated manipulator and its potentials as a clamping and bracing wrist have been presented. The manipulator is featured with two orientation freedoms to adapt to a complex surface and a translation freedom for a clamping actuation. The static analysis, along with the static representation of velocity and force ellipsoids, establishes a rational basis for minimizing the bending moments which tend to cause an increase in nonlinear friction. Also, it predicts the reaction forces acting at the ball joint for a specified payload, which appears as time-varying external forces/moments on the link actuation. The control strategy of actuator characteristic contouring was suggested to approach ideal actuator characteristics depending on task specifications. Future research will be directed towards the experimental investigation.

ACKNOWLEDGEMENTS

The research is supported by the General Research Fund of Georgia Tech.

REFERENCES

1. Lewis, G., 1983, Modular fixturing systems. *Proc. 2nd Int. Conf. on Flexible Manufacturing Systems*, (ed. K. Rathmill), 451-462, London, UK, North Holland Publishing Company.
2. Machine tool makers: healing, but Sickly. 1985,8 *Business Week*, 119-120.
3. Albert, M. 1987, Setup reduction: low cost, big payoff, *Modern Machine Shop*, Nov. 90-99.
4. Asada, H. and West, H., 1984 "Kinematic Analysis and Design of Tool Guide Mechanisms for Grinding Robots," *Computer Integrated Manufacturing and Robotics*, ASME WAM, New Orleans December.
5. Book, W. J., Le, S., and Sangveraphunsiri, V., 1984 "Bracing Strategy for Robot Operation," *Proc. of RoManSy'84: The Fifth CIMS-IFTOMM Symp. on Theory and Practice of Robots and Manipulator*, Udine, Italy, June, pp. 179-185.
6. Kwon D-S. and Book, W. J., 1988 "A Framework for Analysis of a Bracing Manipulator with Staged Positioning," ASME WAM, Nov 27 - Dec. 2, Chicago.
7. Lee, K-M and Shah, D., 1987, "Kinematic Analysis of a Three Degree of Freedom In-parallel Actuated Manipulator," *Proc. 1987 IEEE Int. Conf. R. & A.*, Raleigh. Also in *IEEE J. of R. & A.*, Vol. 4 Issue 2 June 1988.
8. Yoshikawa, T. 1984 "Analysis and Control of Robot Manipulators with Redundancy," Robotics Research: *The First Int. Symp.*, ed. M. Brady and R. Paul, MIT Press, pp. 735-747.
9. Asada, Haruhiko, and Cro Granito, J. A., 1985 "Kinematic and Static Characterization of Wrist Joints and Their Optimal Design," *Proc. 1985 IEEE Int. Conf. R. & A.*
10. Wormley, D. N., Lee, D. and K-M. Lee 1981 "Development of a Fluidic, Hydraulic Servovalve," Final Report HDL-CR-81-216-1, US Army Harry Diamond Laboratories.
11. Wormley, D. N. and K-M. Lee 1983 "Integrated Component Fluidic Servovalves and Position Control System," Final Report HDL-CR-82-158-1, US Army Harry Diamond Laboratories.
13. Hogan, N. 1985, "Impedance Control: An approach to Manipulation: Part I - Theory, Part II-Implementation, Part III - Applications," pp. 1-24 ASME Journal of DSMC Nov. 107.
14. Goldenbery, A.A., 1988 "Implementation of Force and Impedance control on robot Manipulators," *Proc. IEEE Int. Conf. of R. & A.*, April 24-29, Philadelphia.